Thermal Modeling of Resonant Scatterers and Reflectometry approach for Remote Temperature Sensing

Michael Gilch, Nicolas Barbot, Darine Kaddour, Romain Siragusa, Filippo Costa, Simone Genovesi, Etienne Perret, Florian Requena

Thermal Modeling of Resonant Scatterers and Reflectometry approach for Remote Temperature Sensing

Florian Requena, *Student Member, IEEE,* Michael Gilch, *Student Member, IEEE,*
Nicolas Barbot, *Member, IEEE,* Darine Kaddour, *Member, IEEE,*
Romain Siragusa, *Member, IEEE,* Filippo Costa, *Senior Member, IEEE,*
Simone Genovesi, *Senior Member, IEEE,* and Etienne Perret, *Senior Member, IEEE.*

***Abstract*—A thermal modeling of different transmission lines (TLs) based on resonant scatterers is presented. Co-planar strip (CPS) and microstrip (MS) TLs are used to model resonators and to introduce the thermal dependency. A reflectometry approach is employed to validate the model by detecting the scatterers' resonance frequency and by comparing it with analytical expressions. The observable shift in the resonance frequency of the scatterers with temperature variations is due to the thermal expansion of metals and temperature dependence of the substrate permittivity. Since all the measurements are done remotely with no direct line of sight, it is shown how such a reflectometry approach can be used for remote temperature sensing using a passive label composed of resonators. Unlike previous works in this domain where the thermal dependency is considered empirically, the introduced model is used to take into account all thermal effects affecting the resonant scatterers allowing to link rigorously the variations of the measured resonance frequency with the temperature without any lookup table. Temperature sensing using very simple TLs based on resonant scatterers was demonstrated in a real environment. A temperature error of less than 3°C is obtained. Once the temperature has been determined, it is possible to go back to the TL parameters such as the effective permittivity and the physical length.**

***Index Terms*—Radar, Scatterer, Thermal expansion, Wireless sensor.**

I. Introduction

TRADITIONAL radar applications permit the detection of a target presence, position, or velocity. It is composed of one or several antennas able to emit an electromagnetic wave towards the target and to receive the backscattered field. Reflectometry applications based on this principle are also used for identification and sensing. The main difference with traditional radar applications is the use of a known target that has been designed for the specifically requested need. It has been shown that using a specifically designed radar target and a Vector Network Analyser (VNA), several physical quantities can be sensed wirelessly such as temperature [1], humidity [2], gas [3] or, permittivity [4]. Closer to the scope of this paper, contact-less characterization of coplanar strip-line discontinuities by Radar Cross-Section (RCS) measurement has been presented in [5], or contact-less characterization of metals thermal expansion in [6].

In this paper, a reflectometry approach is used to develop a thermal modeling of a TL-based resonant scatterer by introducing the temperature dependence in the line effective permittivity, as well as in its physical length. The resonators are considered as a CPS or a MS line with specific boundary conditions. With this approach, the introduction of the temperature dependence is straightforward: thermal expansion of metals and temperature dependence of the substrate permittivity (which are physical quantities directly linked to the scatterer resonance frequency) can be added in common TL formulas such as the ones describing CPS or microstrip line. In this way, physical insight into the origins of the thermal dependency is kept. Note that this approach is different from the classical one used to model thermal variations in TL [7], [8], where a thermal dependency is considered on the inductive reactance and the series resistance of the transmission line. Contrary to that, the proposed approach uses as inputs the coefficient of thermal expansion (CTE) and the thermal dependency of the substrate which are two physical quantities that are generally provided by manufacturers.

Based on the reflectometry approach, all the measurements are done remotely using one or two antennas (this depends on the mono-static or bi-static configuration considered) and a VNA. Based on the analytical formulas introduced, an approach to extract the temperature is also described demonstrating how the designed scatterers can be used as temperature sensors. The extracted temperature will be compared with the one directly measured with a thermometer for demonstrating the accuracy of the proposed model. Numerous works have been done in the field of chipless RFID for temperature sensing (see Table I). For example, the use of a resonator composed of a substrate with thermal dependent electrical parameters has been widely investigated [9], [1], [10]. The variation of electrical conductivity can also lead to the measurement of the temperature [11], [12].

However, none of these studies have developed an accurate model to link rigorously the measured resonance frequency to

F. Costa and S. Genovesi are with Department of Information Engineering, University of Pisa, 56122-Pisa, Italy

The remaining authors are with Univ. Grenoble Alpes, Grenoble INP, LCIS, F-26000 Valence, France.

E. Perret is also with Institut Universitaire de France, Paris, France.

TABLE I
DIFFERENT APPROACH USED IN CHIPLESS RFID FOR TEMPERATURE SENSING

	[1]	[10]	[12]	[13]	[14]	*
Thermal effect investigated	Change in permittivity	Change in permittivity	Change in conductivity	Dilatation of 3D structure	Change in permittivity	Change in permittivity and dilatation
Sensor design information	Planar shape PCB design	Planar shape PCB design	Planar shape Ink-jet printed	3D cantilever Clean room	Fully dielectric machined	Planar shape PCB design
Presence of ground plane	Yes	No	No	No	No	Depends on the resonator used
Materials considered in the study	Stanyl polyamide	Stanyl polyamide	Polymer carbon nanotube composite ink	Gold and silicium cantilever	Ceramic cylinder	Metallic resonator on a substrate
Measurements in real environment	No	Not mentioned	No	Yes	Yes	Yes
Measurements through obstacles	No	No	No	No	No	Yes
Resonance frequency	0.7GHz	6GHz	2.4GHz	22GHz	2.9GHz	3GHz
Frequency shift / Temperature variation	0.04 GHz / 50°C	Not mentioned	36.9% of RCS amplitude	1.7 GHz / 250°C	0.1 GHz / 220°C	3 MHz / 30°C

* the proposed manuscript

temperature variations by taking into account all the different temperature-dependent RF phenomenon. In this paper, an accurate thermal model of the effective permittivity and line elongation of a CPS and MS line is presented. This model takes into account material expansion and permittivity dependency on the temperature of the substrate while showing that other thermal effects can be neglected. The link among the resonance frequency, the line elongation, and the TL effective permittivity is presented and the temperature dependence is exposed. The variation of the scatterer dimensions and its electrical parameters due to a change in temperature causes a shift of their resonance frequency which can be monitored remotely using a reflectometry approach. Then the use of such a model and scatterers can be applied to the measured resonance frequency for temperature sensing.

The paper is organized as follows, in Section II, analytical expressions used to model the CPS TL effective permittivity and the resonance frequency of the scatterer with temperature are introduced. In Section III and IV, two parameters needed for the model and so for the temperature extraction are presented. Section V to VII present the validation in simulation and measurement of the model for application in temperature sensing. The model of the microstrip resonant scatterer is proposed in Section X. Section XI speaks about the humidity impact on the temperature sensing. Finally, concludes the paper.

II. DESCRIPTION OF THE SCATTERER-BASED CPS TL

The first step to model the temperature effect on a scatterer, as previously explained, consists of treating a resonant scatterer as a TL. The rectangular loop is a good candidate, because an analogy between this simple geometry and a CPS TL section terminated at both ends by a short circuit (SC) can be done [5]. Fig. 1 presents the topology of a classical rectangular loop resonator. In this simple configuration, the resonator is only composed of one layer of metal, without any ground plane or substrate. The geometrical dimensions (l, g, w) illustrated in Fig. 1-a is the nominal dimension used for the fabrication. The metal is thick enough 100μm for the loop to be rigid. The resonator can also be placed on the top of any support, like planar dielectric substrates. Note that in this last configuration, the structure is similar to a more practical CPS TL short-circuited at both ends. With such a metal loop and the possibility to place it on top of any substrate, it is possible to dissociate the effect of temperature on the metallic part of the TL (which will characterize the TL length variation), from the ones relating to the presence of the dielectric. So, based on this, the following methodology will be used: 1) the dilatation of the loop alone will be first characterized. The formula describing the TL length elongation due to temperature variation will be obtained based on the detection of the loop resonant frequency shift. 2) a more complex configuration will be considered: dielectric support with a thermal dependent permittivity will be added to the loop to derive the formula of the TL effective permittivity with temperature dependence. For ease of characterization, the metal loop resonator can be placed on a specific dielectric as already mentioned, or the resonator can also be fabricated like a classical PCB. This second type of fabrication will also be considered for its ease of fabrication.

When a loop at a temperature T is illuminated by an incoming electromagnetic-field, the maximum energy backscattered

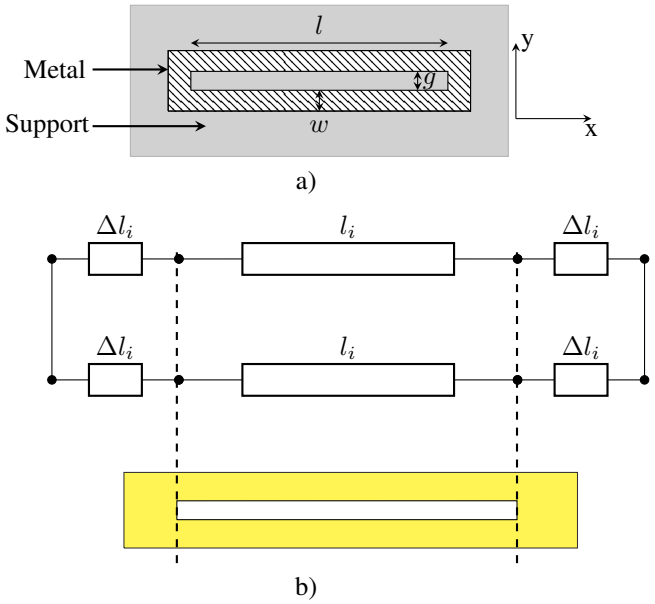

Fig. 1. (a) Nominal dimensions of the fabricated loop (i.e. values used for the fabrication): l=50.83mm , g=2.07mm and w=1.43mm. The polarisation of the electric field used to excite the resonator is along y. (b) Equivalent transmission line model of a loop resonator [5].

occurs at its resonant frequency $f_r(T)$ defined by [5]:

$$f_r(T) = \frac{c}{2\sqrt{\varepsilon_{eff}(T)}(l(T) + 2\Delta l(T))} = \frac{c}{2\sqrt{\varepsilon_{eff}(T)}L(T)} \quad (1)$$

where c is the speed of light in vacuum, $\varepsilon_{eff}(T)$ is the effective permittivity seen by the loop, $l(T)$ is the length of the CPS (which corresponds here to the notch's length) and $\Delta l(T)$ is the additional length taking into account the presence of short circuit (SC) discontinuities as illustrated in Fig. 1-b. It is clear from Fig. 1-b that the loop resonator can be considered as a transmission line section terminated at both ends by a SC [5]. About notations, the effective length $L(T) = l(T) + 2\Delta l(T)$ will be used in the rest of the paper. Two different temperatures will be considered T_1 and T_2, with $T_2 > T_1$. The variation between these two temperatures will be $\Delta T = T_2 - T_1$. Note also that quantities such as $l(T_i)$ or $L(T_i)$ will be noted l_i and L_i respectively to consider their thermal dependency. Physical dimensions of the loop, without any subscript (see Fig. 1) correspond to nominal dimensions. The thermal dependency of all these parameters will be developed in the following part.

III. Thermal dilatation consideration

Thermal expansion of a material is defined as the modification of its volume at a constant pressure with a temperature variation. If we consider a 1-dimension object of length l_1 at temperature T_1 (Fig. 2), this object will expand with an increase of temperature, and the final length at a temperature T_2 is:

$$l_2 = l_1 + d_l = l_1\left[1 + \alpha_{CTE}(T_2 - T_1)\right] \quad (2)$$

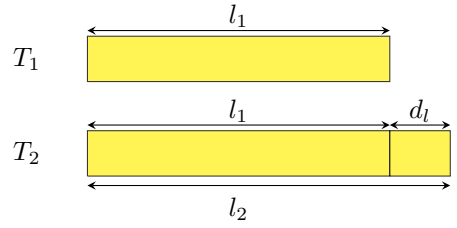

Fig. 2. Expansion of a 1D object due to temperature variation.

where d_l is the expansion in length due to the increase in temperature [15] and α_{CTE} the coefficient of thermal expansion (CTE) of the material.

The effective length L of the resonator variation with temperature can be expressed as [6] :

$$L_2 = L_1(1 + \alpha_c \Delta T) \quad (3)$$

where α_c is introduced as the equivalent expansion coefficient for the effective length.

In the case of the metal loop, the extraction of $\Delta l(T)$ based on simulation as well as the relation between α_c and α_{CTE} have been studied in [6]. Both the value of $\Delta l(T)$ and the relation between α_c and α_{CTE} depend on the loop geometry and the substrate. However, for temperature extraction, we will see that it is acceptable to consider the equality between α_c and α_{CTE}. Indeed in [6] and in Section VII-A, a study of this approximation shows, that only a very small error is introduced, allowing us to adopt the model in the following, even when a dielectric is considered. Note that here, α_{CTE} is defined considering (3) and a temperature of reference T_1 equal to 0°C to use CTE's values obtained from datasheets [16] corresponding to the metals used in this work. Note also that α_{CTE} is supposed to be temperature-independent in the considered temperature range 0°C-100°C. Thereafter, for sake of simplicity in the notations, T_1 is considered equal to 0°C, so ΔT, L_1 (L at 0°C) will be named T and L respectively.

In the following part, the effect of the temperature dependence on the effective permittivity of the CPS is studied.

IV. Temperature dependence of the effective permittivity of the CPS TL-based scatterer

For the loop, the effective permittivity can be modeled by considering again the resonator as a slot line terminated at both ends by SC as illustrated in Fig. 1-b. Thus, the effective permittivity of the loop resonator ε_{eff}, on a single substrate layer, can be expressed as [17] :

$$\varepsilon_{eff} = 1 + \frac{\varepsilon_r - 1}{2} q \quad (4)$$

where ε_r is the permittivity of the substrate. The parameter q is dependent on the thickness of the substrate and the geometry of the resonator as described by the analytical expression given in [17, eq. (21)]. In our case, the permittivity of the support is considered to vary with the temperature following the relation $\varepsilon_r(T) = \varepsilon_r(1 + \beta T)$ where β is the thermal-dependency of

the substrate that can be obtained from material datasheets. Equation (4) can be rewritten as:

$$\varepsilon_{eff}(T) = 1 + \frac{\varepsilon_r(1+\beta T)-1}{2}q \tag{5}$$

Like previously for the effective length L_2 in (3), the effective permittivity can be expressed as:

$$\varepsilon_{eff}(T) = \varepsilon_{eff}(1+\alpha_p^{CPS}T) \tag{6}$$

where the thermal-dependency of the effective permittivity (α_p^{CPS}). The coefficient α_p^{CPS} can be expressed as a function of the thermal-dependency of the dielectric substrate β by using (6) and [17, eq. (21)] as:

$$\alpha_p^{CPS} = \frac{\beta q \varepsilon_r}{2+(\varepsilon_r-1)q} \tag{7}$$

Strictly speaking, like L, ε_{eff} is the CPS TL effective permittivity defined at 0°C.

Concerning the validity range in frequency of the model, it depends on the analytical expressions of the TL used in the approach. Note that (4) can be used up to 100 GHz [17] which shows that the model is compatible with the UWB band (3.1 GHz - 10.6 GHz) which is usually used in Chipless RFID. However, the sensitivity of the approach is also related to the value of the quality factor (Q-factor) of the resonators. The higher the Q-factor, the more accurate the extraction of the resonant frequency and therefore the temperature will be. Also, as the Q-factor decreases with the frequency, the best results will be obtained for the lowest frequencies of the considered band.

In the following section, we will see how based on (1), (3) and (6) the temperature of the loop can be extracted with the measurement of the scatterer resonance frequency.

V. Temperature extraction

The equation of the thermal dependence of the loop resonance frequency can be obtained by injecting (3) and (6) in (1). Thus the resonance frequency f_r at a temperature T is :

$$f_r(T) = \frac{c}{2\sqrt{\varepsilon_{eff}(1+\alpha_p^{CPS}T)}L(1+\alpha_c T)} \tag{8}$$

Where α_p^{CPS} is the thermal-dependency of the effective permittivity and α_c the coefficient of effective dilatation of the loop. Linearizing (8) using a Taylor series for small value of $\alpha_i T$ (since $\alpha_p^{CPS}T$ and $\alpha_c T$ are in the order of 10^{-5} and $T < 100$°C). The following equation can be derived :

$$\begin{aligned} f_r(T) &\simeq \frac{c}{2\sqrt{\varepsilon_{eff}}L}\left[1-(\alpha_c+\alpha_p^{CPS}/2)T\right] \\ &= \frac{c}{2\sqrt{\varepsilon_{eff}}L}(1-\alpha T) \end{aligned} \tag{9}$$

where α is defined by

$$\alpha = \alpha_c + \alpha_p^{CPS}/2 \tag{10}$$

Note that α depends on thermal proprieties of the conductor and the dielectric used to fabricate the scatterer and the scatterer shape as shown in (10).

Using (9), the relation between the resonance frequencies $f_r(T_1)$ and $f_r(T_2)$ for respectively two temperatures T_1 and T_2 is:

$$f_r(T_2) = f_r(T_1)\frac{1-\alpha T_2}{1-\alpha T_1} \tag{11}$$

Note that (11) gives the relation between tag's resonance frequencies (obtained from measurement) and the coefficient α (known value depending on the scatterer shape and the material used) and the considered temperatures T_1 and T_2. So, a simple approach to use this resonant scatterer as a temperature sensor consists in characterizing T_1 and $f_r(T_1)$ one time. Then the measurement of $f_r(T_2)$ will allow to extract T_2 using (11).

It is interesting to note that when the current temperature T_2 has been extracted, all the characteristics of the line can be directly obtained at the temperature under test. Indeed the computation of the effective permittivity $\varepsilon_{eff}(T_2)$ of the TL is computed using (6) with ε_{eff} defined by (4). Then the physical TL length l_2 is extracted using (3) and (11).

It is also interesting to note that the length of the loop does not appear in (11), which means that the approach is valid regardless of the length of the loop and so of the operating frequency from the moment the structure resonates. It is therefore possible to miniaturise the tag by working at higher frequencies if necessary.

This equation permits to explain the different influences of the parameters such as the dependency on the metallic conductor chosen to do the resonator, the dielectric parameters such as thickness, permittivity, thermal dependency, the resonator shape, etc ... It can be used to find optimal parameters to increase the sensibility of a potential sensor: the initial resonance frequency, a conductor who dilates more, dielectric who varies more, etc ..

A. Discussion on Approximations for the determination of the temperature

Temperature variation has a lot of consequences on RF parameters even for the simple TL-based scatterer under study. It is why only the main contributions have been taken into account in the model introduced above. This means that several approximations have been made in order to obtain this model, and the objective of this subsection is to discuss these assumptions. Some of them will be evaluated in simulation in the next section and the entire model will be confronted with measurements to validate its accuracy in the rest of the paper.

1) Thermal Expansion of Dielectric:

Like for the metal part, the substrate volume is not constant with the temperature variation. Dielectrics generally expand with an increase of temperature, and this is observable in the three spatial directions. For needs of mechanical robustness, particularly to ensure temperature robustness, materials used in the manufacture of any item must have similar thermal expansion constants. Otherwise, the object may deform irreversibly or even break. This applies to the manufacture of PCB and electronic packaging. For example the Rogers RO4003C has CTE of 11, 14, 46 ppm/°C respectively in the

x, y, z-axis. The CTE of copper is 17 ppm/°C. Our model integrates the mechanical deformation of the line as a function of temperature. However its origin could be related to the metal as well as to the dielectric. What is important here is to take into account a CTE value representative of this deformation. Taking that of the metal (the latter being slightly higher than the dielectric) leads to results in accordance with the experiments shown in Section VII. This was also confirmed by our approach of treating the metal loop alone and then with the dielectric. It is the same when the loop is simply placed on the dielectric or attached as is the case when the resonator is manufactured as a PCB.

Dielectric elongation can also impact the substrate thickness. In such a case, almost all devise parameters are modified like q or even Δl. However, in the considered temperature range, the thickness variation is low in comparison with the other effects. In the case of Rogers RO4003C, q varies from 0.5828 to 0.5830 for a substrate expansion caused by a temperature variation of 60°C. In this case, α_p^{CPS} goes from 23.738 ppm to 23.744 ppm which is negligible.

2) Electrical conductivity variation with temperature: It is also well-known that the electrical conductivity of any metal varies with temperature. This phenomenon has not been considered in this work for two reasons. In first approximation, electrical conductivity variation will affect only the TL losses and not the TL electrical length. Effects of temperature on losses are not considered in this paper since only the resonance frequency shift is taken into account. Note that the resonance frequency shift can be measured with high accuracy. This is not the case of the magnitude of the signal at the resonance which can be impacted by the presence of surrounding objects around the scatterer.

To characterize TL losses variations with temperature, a simple approach like the one in [7], [8] can be used. The temperature dependence of the line effective resistance can be taken into account using a formula similar to (2) (linear dependence of the resistance with the temperature). The second reason is due to the fact that in the temperature range under study, the variation of the electrical conductivity is small. It will be decreased by a factor of 2 - 3 for an increase of 100°C. These small variations in the electrical conductivity will lead to variations of the magnitude of the RCS that are not significant in relation to the measurement accuracy.

3) Approximations linked to $\Delta l(T)$ and α_c:
As explained in [6], for a metal loop a more general relation between α_c and α_{CTE} is given by :

$$\alpha_c = \alpha_{CTE} \frac{L + K \times \Delta l}{L + \Delta l} \tag{12}$$

where the coefficient K describes the dilatation of the SC discontinuities (see [6, eq. (3)]). Indeed, concerning the SC discontinuities, the temperature effect is not only linked to variations along the line, but also due to variations in the transverse section, which introduces another effect that can be model with the constant K. In this paper dedicated to temperature sensor, the condition K=1 is taken, so α_c and α_{CTE} are considered to be equal. When the scatterer is printed on a dielectric, the relative permittivity has also to be considered in the computation of Δl_1. This dependency is given by the following formula [5] :

$$\Delta l(\varepsilon_{eff}) = \frac{\Delta l}{\sqrt{\varepsilon_{eff}}} \tag{13}$$

So (12) can simply be rewritten considering the presence of the dielectric. The study of the influence of K on the temperature extraction in [6] and in Section VII-A (with or without dielectric) shows that the introduced errors lead to a very small variation which is negligible. Indeed, the measurement errors of the resonance frequencies have higher errors contributions in the extraction of the temperature as shown in Section VII-A.

VI. Simulations

Simulations have been done to validate (2) using CST. CST thermal and mechanical solvers are first used to impose the desired temperature on each point of the loop given in Fig. 1-a by considering a constant ambient temperature. The initial loop dimensions given as input in the simulation are the ones noted in the caption of Fig. 1-a. These dimensions are considered to correspond to temperatures in the range 0°C-60°C with a 5°C step. The simulation in CST MW uses a plane wave excitation and the Time Domain Solver. The loop is in free space and is made with copper so that $\alpha = \alpha_c = 17 \times 10^{-6}$°C^{-1}. The simulated RCS is plotted in Fig. 3. By increasing the temperature, the TL length increases so the resonance frequency decreases as stated by (9). A total frequency shift of 3MHz is observed for the 60°C variation with an initial resonance frequency of around 2.98 GHz at 0°C. Fig. 4-a presents the evolution of the resonance frequency versus the simulated temperature. By applying (11) on the simulated resonant frequencies f_r, we can plot the extracted temperature as a function of the one imposed in simulation (Fig. 4-b). Extracted temperature is very close to the imposed one with a maximum error below 0.1°C over the 0°C-60°C temperature range.

To study the effect of K on the extracted temperature, a loop of dimensions l=38mm is considered. Following Section III, this loop is characterized by a value of K equal to 0.91. If we approximate K=1 to simplify the expression of α_c, the extracted temperature using (9) is plotted in Fig. 5. The error is less than 0.5°C on a 0-60°C temperature variation. The linearity in the error comes from the error in the linear coefficient of (10) since K was approximated in α_p^{CPS}. The maximum temperature variation, measured in an office (considered here as an example of a real sensor application in Session IX), was of 6°C. In this case, due to the approximation K=1 (rather than considering the exact value 0.91), the maximum error introduced on the estimated temperature is only of 0.03°C. So, compared to the resonator used in Session IX (l=51mm and K=1.02 without any approximation), the difference between K=0.9 and 1 is higher and so introduces more errors than the case used in practice. For these reasons the approximation K=1 was assumed to be suitable for the application and for the loop resonators.

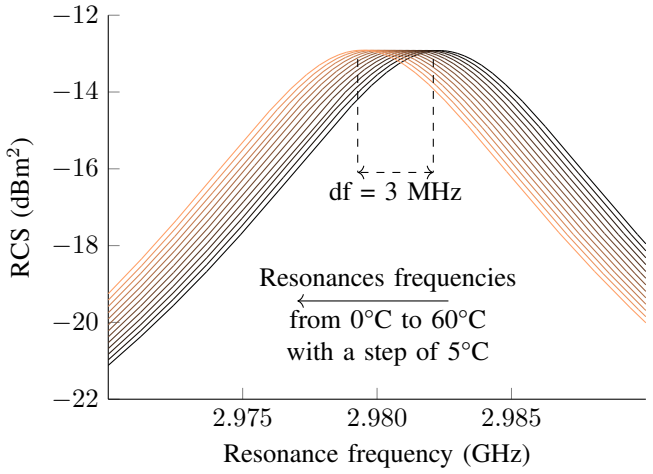

Fig. 3. RCS as a function temperature for the simulated copper resonator in vacuum for temperature ranging from 0°C to 60°C with a 5°C step.

The case of a non-thermal dependent support ($\beta = 0$, $\varepsilon_{eff} \neq 1$) has also been studied to see the effect of the permittivity of the support on the extracted temperature. The same loop described in Fig. 1 is simulated on a 50mm thick dielectric of permittivity constant ε_r ranging from 1 to 5. Fig. 6 plots the error between the extracted temperature and the simulated one. The coefficient α_c is calculated with $K = 1.02$, ε_{eff} is obtained with [17] and $\Delta l(\varepsilon_{eff}) = \dfrac{\Delta l}{\sqrt{\varepsilon_{eff}}}$ [5]. The error on the extracted temperature is very low (less than 0.2°C) thus validating the possibility to use such a substrate in our model.

Finally, the general case of a support with a temperature dependency of the dielectric constant has been studied to validate that both conductor and dielectric thermal effects were correctly considered in (9). In this last configuration, the simulated temperature sensor tag is supposed to be fabricated with PCB technology. The loop is in copper ($\alpha_{CTE} = 17 \times 10^{-6}$°C^{-1}) on a RO4003C substrate with a dielectric constant of 3.55 with thermal dependency $\beta = 40 \times 10^{-6}$. The substrate thickness is 1mm which leads to a value q = 0.58 [17]. Simulation results are plotted in Fig. 7.

The extracted temperature is in good agreement with the imposed temperature with an error of less than 0.7°C. The linearity in the error comes from an error in the linearity in (11) on the value of α. The calculated α using (11) is 25.5×10^{-6}°C^{-1} while a value of 25×10^{-6}°C^{-1} (equivalent to q = 0.53) leads to lower error of less than 0.45°C. Henceforth, these results demonstrate that (9) is accurate enough to model thermal effects on the resonance frequency of the loop.

VII. Evaluation of the Error

A. Uncertainty

The uncertainty of the method can be estimated with (11) using :

$$\Delta T = \left|\frac{\partial T}{\partial f(T_1)}\right| \Delta f(T_1) + \left|\frac{\partial T}{\partial f(T_2)}\right| \Delta f(T_2) + \left|\frac{\partial T}{\partial \alpha}\right| \Delta\alpha \quad (14)$$

with Δf = 10kHz (VNA accuracy) and $\Delta\alpha = 1 \times 10^{-5}$ (corresponding to 5% error on the calculated α).

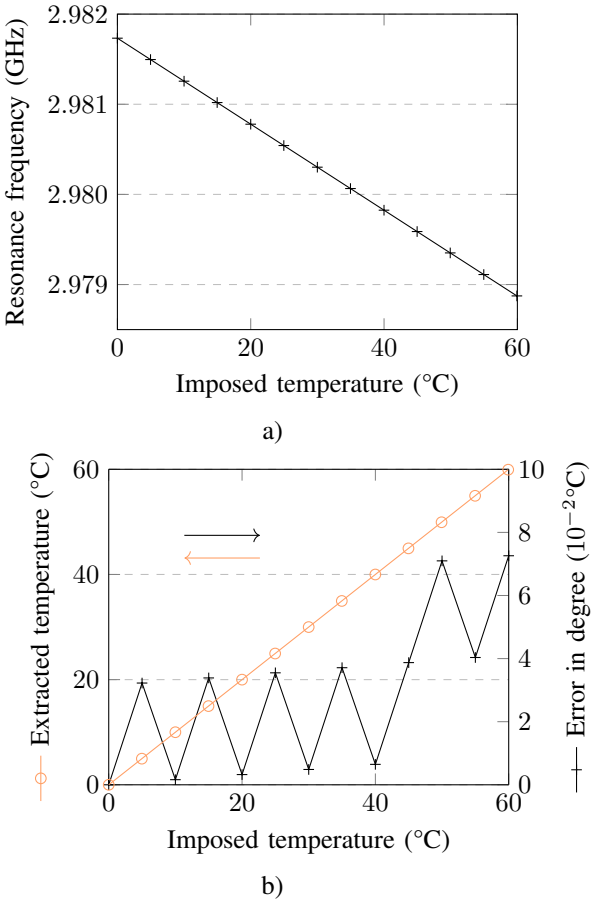

Fig. 4. (a) Resonance frequency in GHz of the copper loop resonator in vacuum as a function of temperature. (b) Extracted temperature using (11) and error in °C.

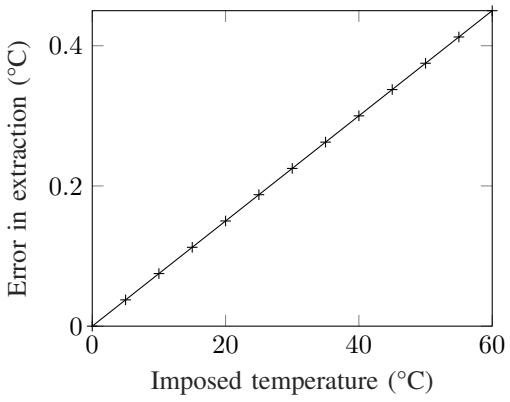

Fig. 5. Error between the extracted temperature using (11) and the simulated temperature when the approximation K=1 is used.

If we do the numerical application where T is given by (11) using $\Delta f = 10kHz$ and $\Delta\alpha = 10^{-5}$, we can see that errors in the measured frequencies Δf_i introduce uncertainties 10 times bigger than error $\Delta\alpha$ on the coefficient α but overall, the uncertainty is low (around 3°C) which explains the good agreement with our results in practice.

In practice since each resonator can estimate the temperature, sensing and averaging on all the resonators can increase the robustness of the sensor without impacting the

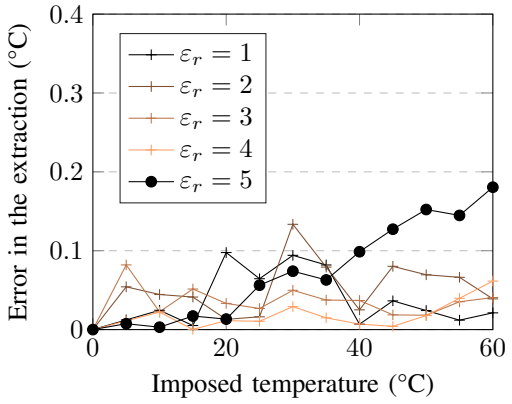

Fig. 6. The error in the extracted temperature of (11) in °C as a function of the simulated temperature with 0°C as a reference measurement for a copper resonator on a 50mm thick support whose permittivity is ranging from ε_r = 1 to 5.

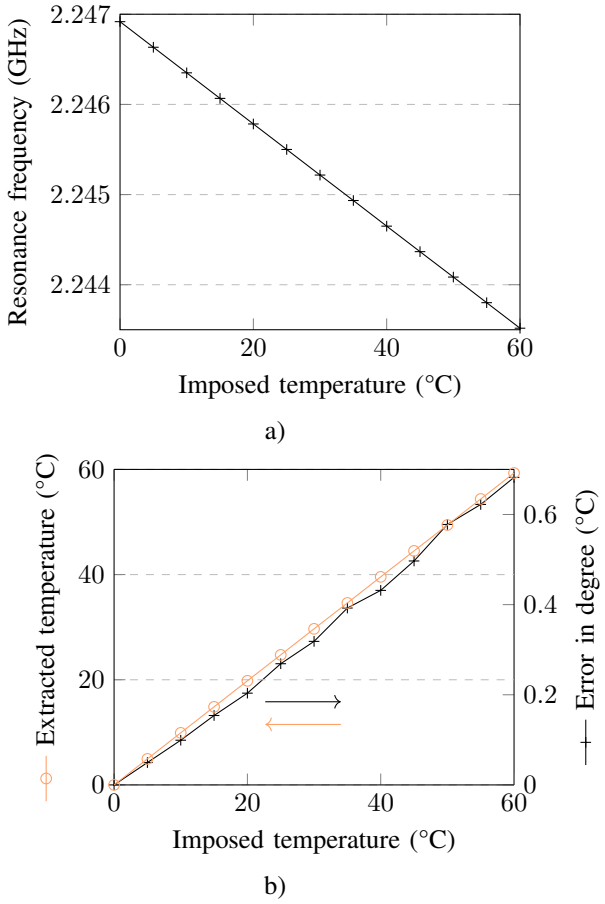

Fig. 7. (a) Resonance frequency of the copper loop on a temperature dependent support (RO4003C) of 1mm thickness (q=0.58) as a function of temperature. (b) Extracted temperature with (11) and error in °C.

identification functionality.

B. Sensitivity of the sensor

The resonance frequency shift due to temperature at the n-th harmonic of a resonator can be computed using (9) and is

$$df_n = \alpha \Delta T \frac{nc}{2\sqrt{\varepsilon_{eff}}L} \tag{15}$$

Thus, to improve the sensibility of our sensor, we have to increase the frequency shift. To achieve this, we can :

- Increase the coefficient $\frac{c}{2\sqrt{\varepsilon_{eff}}L}$ which result in a more compact resonator resonating at only higher frequencies.
- Increase the factor n. We can keep actual dimensions for the ID functionality and do a measurement on a harmonic for the sensor functionality.
- Increase the factor α which means use a metal that expands more (like zinc) and/or a support whose permittivity is more affected by thermal variation β. A totally different geometry of resonator can also contribute in increasing α_p and so α as shown in Section X.

The frequency shift df due to temperature for a given resonance frequency can be computed using (15) and compared with previous simulation results. In the case of the copper loop, the calculated shift is 3MHz which is in good agreement with the simulation results shown in Fig. 3.

Note that the frequency shift due to temperature is small enough to be compatible with the use of this type of scatterer to realize chipless RFID tags for identification purposes [18]. This numerical application shows that the sensing capability can be added to this type of chipless RFIDs tag without any compensation. Indeed this frequency shift has no impact on the ID capability of a chipless RFID tags that encode data using a frequency position technique [18] where a frequency band of few tens of MHz is generally allocated to each code.

As mentioned in the introduction, several papers have been published using the variation in permittivity to sense the temperature (see Table I). However, this approach does not consist in proposing a model of the thermal phenomenon but rather a lookup table that allows linking the measured resonance frequency to a temperature value. This lookup table is obtained after a first practical characterization, in temperature, of the tag. With the proposed approach it is possible to dissociate the variation coming from the dielectric permittivity change from the variation coming from the material elongation. Contrary to what is claimed in most chipless RFID papers on this topic (see Table I – planar / PCB configurations) where only the contribution of the permittivity variation is considered, it should be noted that it is not possible to neglect the contribution of the elongation of the metallic parts as a function of temperature. This is particularly true for scatterer-based CPS TL, and also true to a lesser extent for scatterer-based microstrip TL as it will be discussed in Section X. Equations (10) and (15) show that the shift in frequency is due to the factor $[1-(\alpha_c+\alpha_p/2)\Delta T]$.

Since both terms α_c and α_p usually have the same magnitude, the shift in frequency caused by the metal dilatation is twice more important than the shift caused by a change in permittivity since it is divided by 2. This is amplified if the support is of small thicknesses. In this case, the coefficient q used to calculate α_p^{CPS} is around 0.5 so the thermal dielectric effect can be divided by 4. For example, the factor α of a zinc loop resonator with support with no thermal dependency is $\alpha = \alpha_c = 31 \times 10^{-6}$ while a copper loop resonator on a 1mm thermal dependent dielectric like Rogers RO4003C has

a factor $\alpha = \alpha_c + \alpha_p^{CPS}/2 = 29 \times 10^{-6}$. Hence, a single metallic resonator with no support can have more thermal sensibility than a resonator with a thermal dependent substrate. Most of the time, material elongation is neglected in existing works. Current studies are essentially focused on the choice of a dielectric that is as sensitive as possible to temperature, i.e. with the highest coefficient β.

C. Impact of the distance

To conclude on the evaluation of the errors related to the implementation of this reflectometry-based approach, we will study in this section the impact of the measurement distance on the temperature extraction. The resonator was placed on a guiding rail in an anechoic chamber. The S-parameters were measured with a VNA for different spacings between the tag and the antenna (bi-static configuration) by using the rail to stay in line. Fig. 8-a shows the impact of the distance between the tag and the antennas on the resonance frequency. A resonance frequency shift of 0.4 MHz is measured for a distance variation from a 3 cm to 1 m as illustrated in Fig. 8-b. By using (15), this frequency shift corresponds to a change of around 4°C. This error of 4°C can have two origins. First when the distance increases, the backscattering signal becomes lower, and it is possible that part of the variation is due to the measurement itself. The second origin can be explained by the variation of the temperature inside the anechoic chamber due to the presence of an operator who has to enter into the chamber to change the position of the tag. Considering this second effect, we can admit that an error on the temperature extraction of 3°C, as computed in Section VII.A, can still apply for a measurement range from 3 cm to 1meter. This possible error of 4°C will have no effect on the measurement. Indeed, in (11), the reference measurement will act as a calibration so if the tag is not moved during measurement, no additional error will be added. This idea will be demonstrated in practice using different reading ranges.

In the sections VIII and IX, the measurement benches used to validate the temperature extraction are described. The first set of measurements (Section VIII) focuses on the validation of the model developed in this paper for various tags configuration in a controlled environment. The second measurement (Section IX) emphasizes the sensor application of this paper where a low-cost traditional PCB design is used in a real environment to sense temperature.

VIII. Temperature Sensing in a Climate Chamber

The model developed in (9) will be first validated in a controlled environment. Several resonators with the same geometric dimensions presented previously in Fig. 1-a have been fabricated using different metals such as Zinc, Copper, and Nickel. In such configuration no dielectric support is used. CTE of these different metals provided by our metals' provider Goodfellow [16] for a temperature range 0°C-100°C following ASTM or DIN test methods are reported in Table II. Copper resonators on a Rogers RO4003C dielectric and a zinc loop put on a high temperature-dependent dielectric (K50)

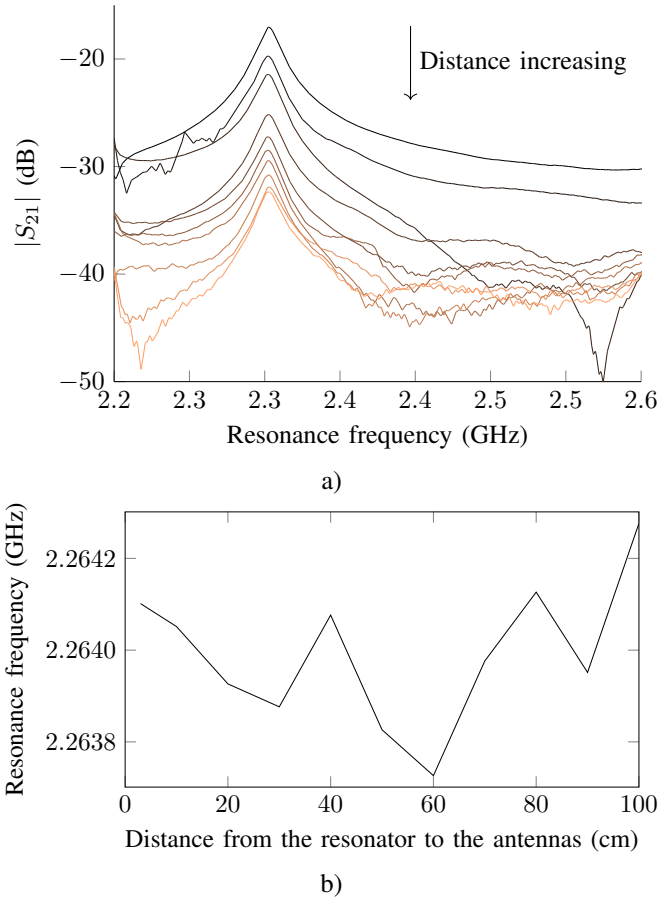

Fig. 8. (a) Effect of the distance on the S-parameters amplitude. (b) Effect of the distance on the resonance frequency.

have been also fabricated to take into account the support thermal dependence. The dielectric and thermal properties of RO4003C and K50 are listed in Table III. The main characteristics of the Rogers RO4003C substrate are given in [19]. It can be seen that the evolution of the dielectric constant is linear regarding the temperature over the range -50° to 150°C. For K50, the characterics can be found in [20]. This panel of 5 resonators has been selected to prove the validity of (9) for different materials and with or without support.

A. Measurement setup

The measurement setup used in a climate chamber and the fabricated scatterers operating as temperature sensors are illustrated in Fig. 9.

A climatic chamber VC0018 by Votsch is used to control the temperature. Absorbers are placed inside the chamber to reduce the reflection level. A bi-static antenna configuration is used to increase isolation (see Fig. 9-a). The measurement protocol is the following: the temperature in the climatic chamber is first set. When the temperature is stabilized, the S_{21} parameter is measured using a VNA. To increase the accuracy on the temperature measurement, the temperature of the loop is then determined using a thermal camera (Infrared Thermal Camera TC-1). Indeed this method is used to be confident on the measured temperature because of the thermal inertia of

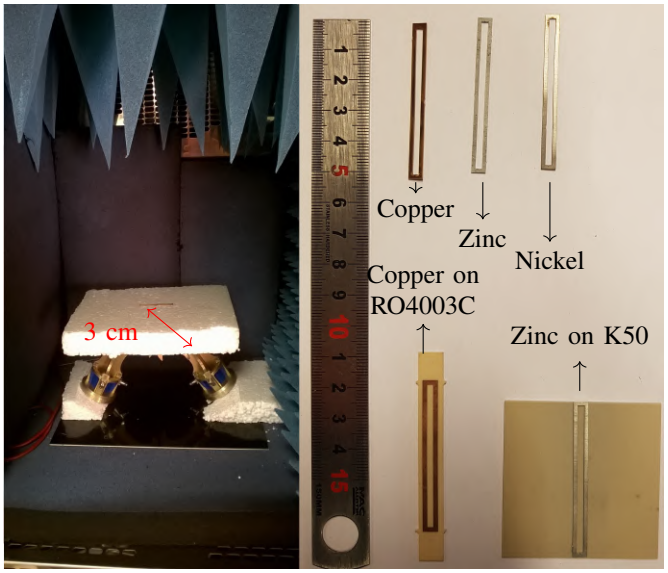

a) b)

Fig. 9. Setup configuration : (a) Setup inside the climatic chamber. (b) The loop resonators made with different metals.

TABLE II
CTE FOR DIFFERENTS METALS [16]

Metal	Thermal expansion coefficient ($°C^{-1}$)
Zinc	31.0×10^{-6}
Copper	17.0×10^{-6}
Nickel	13.3×10^{-6}

TABLE III
RF AND THERMAL CHARACTERISTICS OF RO4003C (ROGERS) AND K50 (NATIONAL MAGNETICS GROUP) DIELECTRICS

Dielectric	RO4003C	K50
Permittivity	3.55	50
Permittivity thermal dependance (β)	40×10^{-6}	-700×10^{-6}
Thermal dilatation ($10^{-6}°C^{-1}$)	X=11, Y=14, Z=46	9.7

the different materials inside the cavity. A first measurement is done without the resonator. After that the resonator is put in its place and the first measurement is subtracted to the new measurements to remove the response of the environment. The resonance frequency of each temperature is extracted and (11) is applied to extract the temperature based on the RF measurements.

B. Results and analysis

With (11), the temperature can be extracted from the measured resonance frequency. The extracted temperature and the error with the temperature measured with the infrared thermal camera (noted expected temperature in the following) are plotted in Fig. 10 for the zinc resonator. We can see that the maximum error is 1.8°C at 31°C. Everywhere else the error is lower than 1°C.

Temperature extraction using (11) is applied for the rest of our 5 scatterers and results are shown in Table IV. The highest error is for the zinc loop with an error of 1.8°C. On average, the extracted temperature error is lower than 1°C. Copper resonator has the best results both with respect to the maximum error and the average error.

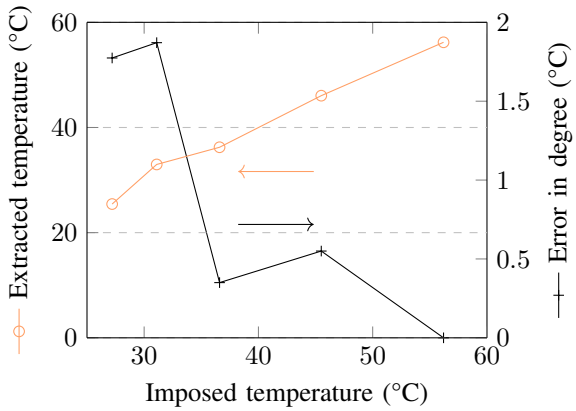

Fig. 10. Extracted temperature using (11) in measurement on the zinc resonator and the error done with the measured temperature in the climatic chamber - the reference temperature is T_1 =56.6°C.

TABLE IV
TEMPERATURE EXTRACTION USING (11) FOR DIFFERENT SETS OF MEASUREMENTS

Set	Max error (°C)	Average error (°C)
Zinc	1.8	0.9
Copper	0.24	0.15
Nickel	1.39	0.46
Zinc on K50	1.60	0.58
Copper on RO4003C	0.89	0.44

IX. TEMPERATURE SENSING IN A REAL ENVIRONMENT

The PCB scatterer composed of a copper loop on a RO4003C substrate is the one used in this section. The resonator is shown in Fig. 9-b. The presence of a thermal dependent dielectric increases the frequency shift (so the accuracy as mention in Section VII.B).

A. Measurements

Four test-benches in a real environment were built and used to validate the potential of the scatterer for temperature sensing applications (Table V). The principle of the test-bench is illustrated in Fig. 11. The PCB tag is placed on a support of thickness t at a distance d from the antenna(s). Both monostatic and bi-static antenna configurations were tested. Measurements were performed in different places such as in corridors, offices. Some places were air-conditioned, some were not. The support was either polystyrene ($\varepsilon_r \simeq 1.1$) to simulate a spacing with air or wood/glass when the measurement was done between two-rooms for example. All these parameters are summarized in Table V. A program running on a computer was measuring every minute the S-parameters of the VNA. The computer was controlling also the measurement of the temperature using an integrated temperature sensor

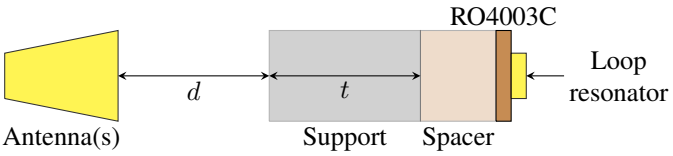

Fig. 11. Principle of the measurement setup in a real environment.

TABLE V
PARAMETERS OF THE FOUR TEST-BENCHES

Measurement set	Antenna configuration	d	t	Support type
1	mono-static	0cm	3cm	Polystyrene
2	bi-static	0cm	12cm	Polystyrene
3	bi-static	10cm	4cm	Wooden door
4	bi-static	10cm	5mm	Glass

(TES 1365). Measurements through a window glass and a wooden door were achieved from one room to another. The test-bench used with the wooden door is shown in Fig. 12 as an example. For the wooden door and glass measurements, a spacer in polystyrene of 2cm was used between the tag and the object (see Fig. 11). An empty measurement of the environment is first done. After that, we subtract this empty measurement to the next measurements to remove as much as possible the environment noise (door impact, glass impact, ...). In all cases during the temperature monitoring, the first measurement was used as a calibration (measurement at T_1) and the tag was not moved during the measurement. For the wooden door and glass measurements, a spacer in polystyrene of 2cm was used between the tag and the object (see Fig. 12). This spacing isolates the tag from the object so that the two elements are not coupled. Therefore, the evolution of the resonance frequency, particularly as a function of temperature, remains independent of the object on which the tag is placed. Indeed, from [17] it is possible to calculate the thickness of the separation layer (spacer) allowing a sufficient isolation between the tag and the object on which the tag is attached. For example, if we consider the following constraining case, namely the stacking of layers: 1) tag dielectric support, 2) metallic layer, 3) air spacer of 5mm and 4) an unknown object (door) potentially of infinite thickness. In this case, the coefficient that multiplies the dielectric permittivity of the different layers q can be computed, and as a result, the effective permittivity is composed at 96% of the first layer dielectric constant (air in this example), and 4% of the second (object on which the tag is attached). So, the influence of an object like a door (in wood or in plastique) will be negligible compared to the others dielectrics. This result is confirmed in practice.

B. Results and analysis

Extracted temperature results are plotted from Fig. 13 to Fig. 16. For the four test-benches, the temperature using the integrated temperature sensor and the one extracted from the loop resonator response with (11) are in good agreement.

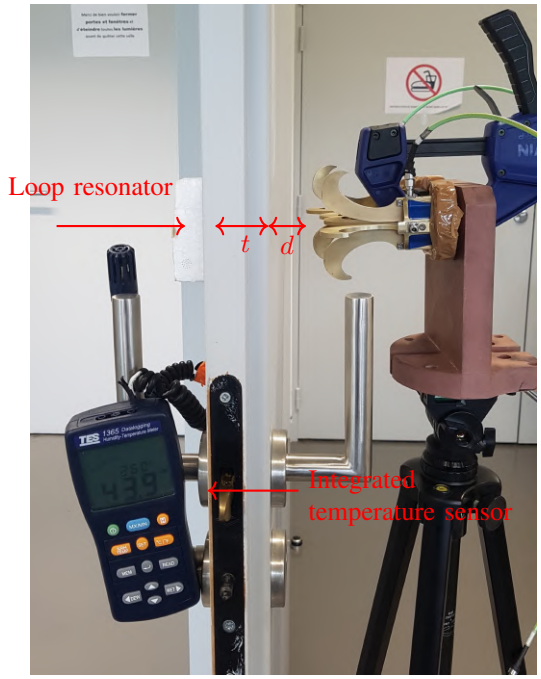

Fig. 12. Principle of the measurement setup in a real environment through a wooden door from a room to another.

In Fig. 13, temperature variations corresponding to daytime/nighttime can be seen. The maximum difference between both measurements is around 2°C on the 3 days measurement duration. To increase the isolation between the incident and reflecting wave and to reduce the error, bi-static measurements are then considered. Bi-static measurements through 12cm of polystyrene and through a wooden door give a maximum error of 0.5°C (Fig. 14 and 15). Bi-static measurement through a window glass gives a higher error of 1.5°C (see Fig. 16).

In Figs. 13 and 15, we can see in practice what was announced in Section VII about the effect of the distance on the measurements: the distance variation is not impacting the accuracy of the temperature extraction.

Another noticeable point is the importance of the frequency resolution (number of points for a given frequency span) for the sensor sensitivity. For test-benches with polystyrene (test-bench n°1 and n°2), a frequency resolution of 10kHz was used. This value corresponds to a temperature sensitivity of 1/9°C as stated by (15) which is observable in the results. For measurements from one room to another (test-bench n°3 and n°4), a lower frequency resolution of 30kHz was used. The corresponding temperature sensibility is 1/3°C as stated by (15) which is also what was measured in practice. This result points out a limiting factor in temperature sensing with this RF approach which is a temperature resolution directly linked to the frequency resolution of the RF equipment used for the measurement.

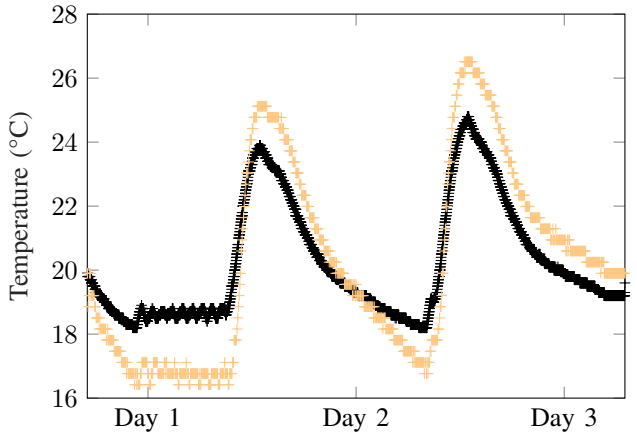

Fig. 13. Comparison between the temperature measured with an integrated sensor in black and using the loop resonator in yellow during a weekend for the test-bench n°1.

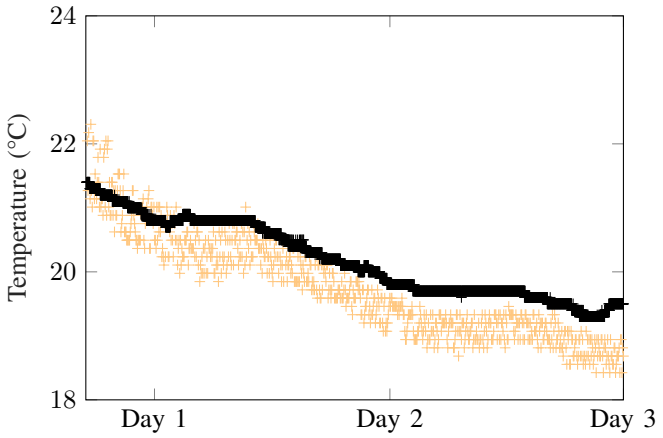

Fig. 14. Comparison between the temperature measured with an integrated sensor in black and using the loop resonator in yellow during a weekend for the test-bench n°2.

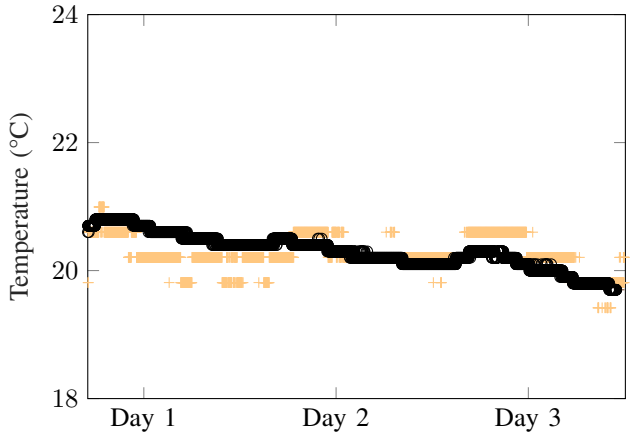

Fig. 15. Comparison between the temperature measured with an integrated sensor in black and using the loop resonator in yellow during a weekend for the test-bench n°3 (Wooden door).

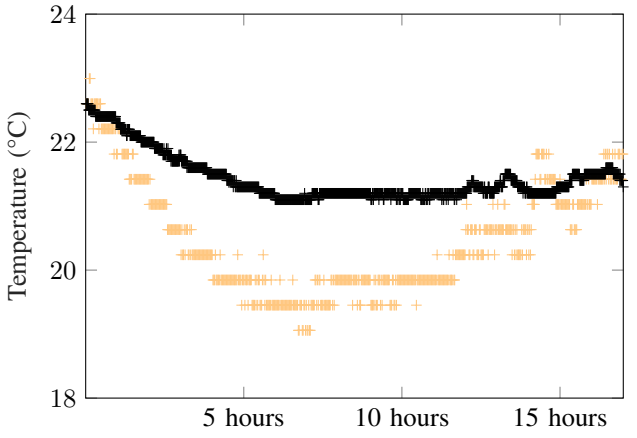

Fig. 16. Comparison between the temperature measured with an integrated sensor in black and using the loop resonator in yellow during a weekend for the test-bench n°4 (Glass).

X. Thermal Characterizations of a Resonant Scatterer-Based Microstrip TL

The same concept can be applied to different types of scatterers. In this section resonant scatterer-based microstrip TL is considered. In its simplest form, the scatterer is a metallic strip (a dipole) above a ground plane. This scatterer can be considered as a microstrip TL section terminated at both ends by an open circuit (OC). This resonator is illustrated in Fig. 17. This resonator offers multiple advantages for temperature sensing. Indeed, the presence of a ground plane confines the electromagnetic fields in the substrate. We will see that in such a case the sensitivity of the sensor can be increased compared to scatterer-based CPS TL when a temperature-dependent substrate is used. Moreover, the ground plane isolates the scatterer from its direct environment, so a spacer as the one used in Fig. 12 is not needed. The major drawback of this resonator is its low Q-factor compared to the loop, leading to a wider peak resonance which makes it harder to find the peak apex corresponding to the resonance frequency. About the thermal dependency of the resonance frequency, the expansion due to temperature can be modeled exactly like the loop. So (2) can be used such as the equality between α_c end α_{CTE}. The thermal-dependency of the effective permittivity α_p^{MS} can be obtained following the same approach introduced in Section IV, i.e. in this case by modeling the dipole over a ground plane as a microstrip line. Note that this OP line is similar to a patch antenna which has been widely studied in the literature [21]. So the classical expression of its effective permittivity can be used and the dependence with temperature can be added. The coefficient α_p^{MS} can then be expressed as:

$$\alpha_p^{MS} = \frac{\frac{\varepsilon_r \beta}{2}\sqrt{1+12\frac{h}{W}}}{\frac{\varepsilon_r+1}{2}+\frac{\varepsilon_r-1}{2}\sqrt{1+12\frac{h}{W}}} \tag{16}$$

where h is the thickness of the substrate and w the width of the dipole as shown in Fig. 17. Considering the scatterer-based microstrip TL geometry given in Fig. 17, a value of

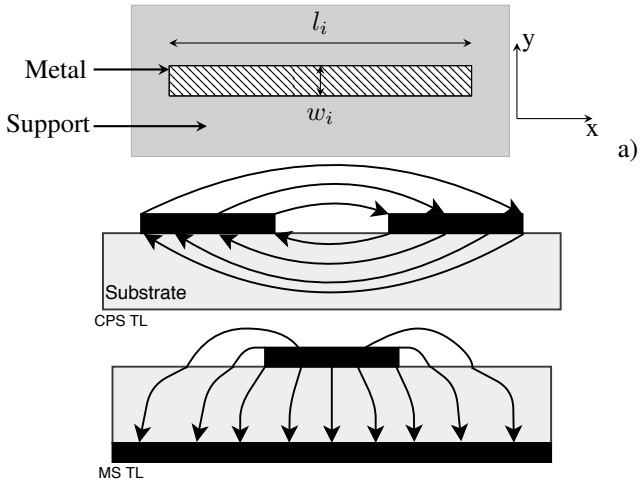

Fig. 17. (a) Resonant scatterer-based microstrip TL. Below the dielectric support of height h a ground plane is placed. Nominal dimension are w=2mm, l_1=2.5cm, l_2=2.2cm and l_3=2cm for the three resonators respectively. The polarisation of the electric field used to excite the resonator is along x. (b) Electric field configuration for the two different TL resonators.

$\alpha_p^{MS} = 23.6 \times 10^{-6}$ is obtained with (16).
Note that in the case of the scatterer-based CPS TL shown in Fig. 1, where $\alpha_p^{CPS} = 22.4 \times 10^{-6}$ was obtained with (7) for the same substrate, α_p^{MS} has a higher value. This is due to the presence of a higher confinement of the fields in the thermal-dependent substrate for the dipole (see Fig. 17).

So, by using the same metal and same substrate as the loop, the dipole over the ground will have a greater frequency shift.

Even in this TL configuration, the coefficient α_c is not negligible in the frequency shift response to temperature and should be considered as stated in Section VII.

A. Measurements

In this measurement, a chipless RFID tag composed of three dipoles over a ground plane is studied [18]. This measurement will show that the proposed model can be generalized to other types of the resonator, as well as the possibility to implement the temperature sensing to existing chipless RFID tags without impacting their identification capability. The measurement protocol is the same as in Section IX-A and test-bench is shown in Fig. 18. A cross-polarisation measurement is done. The 3 microstrip dipoles have respectively a resonance frequency of 3.1, 3.7 and 4.1GHz.

B. Results and analysis

Extracted temperature results are plotted in Fig. 19 alongside the integrated sensor results in black. Extracted temperature using (11) and (16) is in good agreement with the one measured with the integrated sensor. The highest error is of 2°C for the resonator n°2 during the whole measurement validating the analytical thermal model proposed in this paper. We can also see in Fig. 19 that having multiple resonators permits to have multiple independent temperature extraction that can be averaged to increase the robustness of the temperature sensor compared to the utilization of a single resonator. An

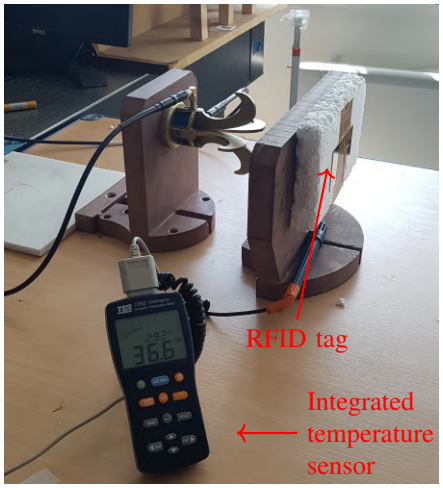

Fig. 18. Principle of the measurement setup for a chipless RFID tag composed of three dipoles over a ground plane thought a wooden object.

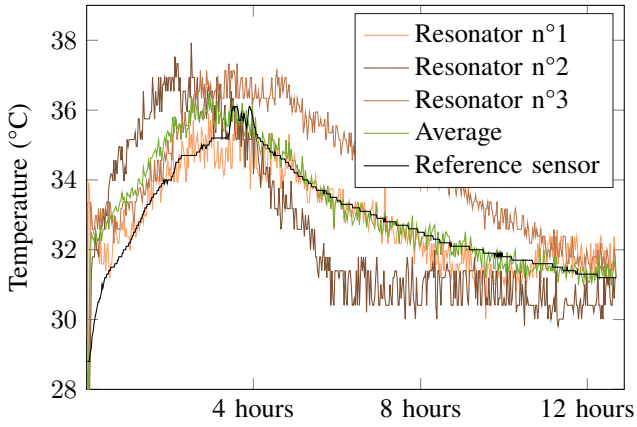

Fig. 19. Comparison between the temperature measured with an integrated sensor in black and using the different resonators that compose the RFID tag.

error of 2.7% is obtained when the averaging temperature is considered.

If we compare the temperature extraction errors between the two types of resonators used (the scatterer-based CPS TL and MS TL), we observe that despite the relation $\alpha_p^{MS} > \alpha_p^{CPS}$ we obtain similar errors in practice. This can be explained by the fact that the measurement accuracy is also related to the quality factor of the resonators. Indeed, as said in section IV, the higher the quality factor, the more accurate the extraction of the resonance frequency and therefore the temperature will be. Here the quality factor of the scatterer-based MS TL resonator is lower than the CPS TL resonator resulting in a better and more robust measurement of the resonance frequency (maximum of the S-parameter curve) for the CPS TL resonator. The measured copper resonator Q-factor is of 148 while the Zinc resonator has a Q-factor of 48 (3 times lower).

It is also important to note that the shift in frequency is not only linked to α but also to the resonator length L, the substrate permittivity and other parameters as shown in (15). A figure of merit based on (15) can be introduced to better

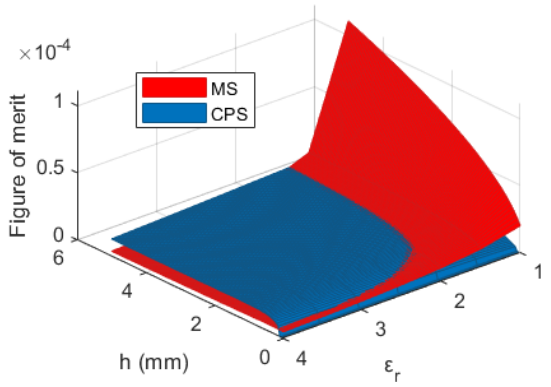

Fig. 20. Figure of merit $\frac{\alpha}{\sqrt{\varepsilon_{eff}}}$ for the CPS and a MS TL-based scatterer as a function of the substrate height h and permittivity ε_r.

illustrate the temperature sensitivity of the resonators under study:

$$\frac{2Ldf_n}{cn\Delta T} = \frac{\alpha}{\sqrt{\varepsilon_{eff}}} \tag{17}$$

This figure of merit can be used to compare different resonator shapes working at the same frequency (same L). If we consider a CPS and a MS TL-based scatterer, we can compute (17) for different dielectric heights h and dielectric constant ε_r to see which one is more sensitive to the temperature. This figure of merit is plotted in Fig. 20. We can see that the sensitivity of the sensor $\frac{\alpha}{\sqrt{\varepsilon_{eff}}}$ is actually lower for the scatterer-based MS TL-based scatterer than for the scatterer-based CPS TL in our configuration (h and ε_r) while presenting $\alpha_p^{MS} > \alpha_p^{CPS}$. The MS TL has a figure of merit of 5.9×10^{-6} while the CPL TL has a figure of merit of 1.7×10^{-5} (almost 3 times higher).

XI. Humidity Effect

Temperature variation in the environment can also significantly change the relative humidity. Such humidity variation can have an impact on the temperature extraction using the proposed model. Indeed, as water's real part of permittivity is around 80 near 3GHz, a higher humidity can lead to a lower resonant frequency due to the increase of the effective permittivity seen by the resonator.

First measurements were done in a climatic chamber where the humidity was maintained constant. These measurements results allowed to validate the introduced thermal behavior. Secondly measurements were done in a real environment where humidity varied during the measurement. These variations (not taken into account in the model) impacted the temperature extraction by adding errors to it. However, it is possible to investigate the humidity impact for a possible real environment application of this type of tag sensors.

By using the climatic chamber presented above, a variation of humidity at constant temperature was performed to characterize the humidity impact on the measured resonance frequency. The measurement results are plotted in Fig. 21.

We can see that a 20% relative humidity variation (from 40%RH to 60%RH) leads to 0.5 MHz shift on the resonance frequency. So by using (15), this shift (linked to a change

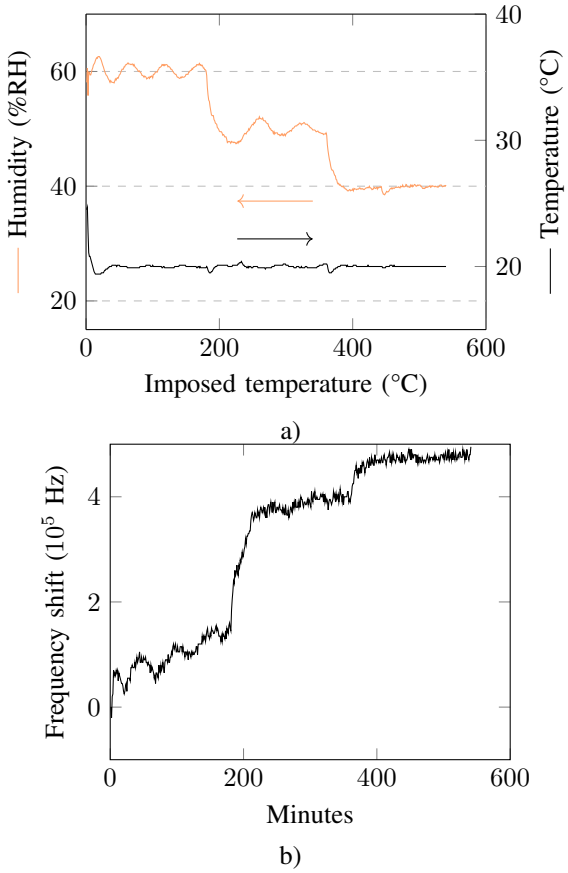

Fig. 21. With significant humidity variation (around 15%HR of change). (a) Measured and extracted temperature. (b) Corresponding resonance frequency variations.

of 20% of the relative humidity) can be seen as a variation of 0.25°C/%RH. Always based on results given in Fig. 21, the introduced error by considering a variation from 50%RH to 40%RH is lower: the shift is only of 0.1MHz which corresponds to a variation of 0.1°C/%RH. Indeed, as shown in [22], the higher the relative humidity, the more the resonance frequency varies. We can extrapolate an error of 0.06°C/%RH for the humidity range 40%-30%RH and 0.0033°C/%RH for the range 30%-20%RH. Concerning the highest humidity values we had during our measurement in real environment, a variation between 40%RH and 42%RH was observed, hence an error of 0.1°C/%RH can be considered in such a case. So, the error on the temperature due to the variation of humidity can be estimated to a maximum of 0.2°C. In the other measurements, a relative humidity lower than 40%RH (even lower than 30%RH in some) was observed, hence the introduced errors are even smaller.

An additional measurement was done in a real environment using the Rogers loop and the results are plotted in Fig. 22. A variation of 7°C was achieved using a heater and a variation of 16%RH was observed. The difference between the extracted measurement and the temperature obtained with a sensor is quite low. Note that the measurement was taken in an office where several people were present during the measurement. Some spikes observed on the extracted temperature could be explained by this highly variable environment near the sensor

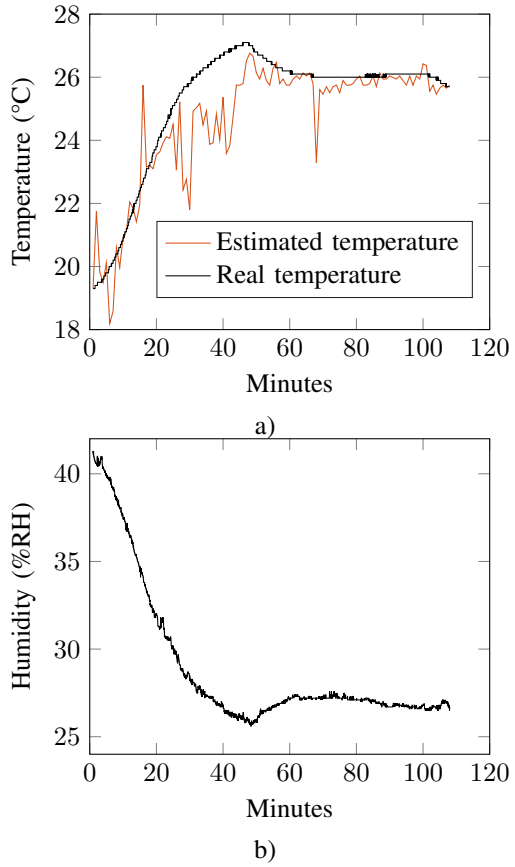

Fig. 22. Temperature measurement in a real environment with big humidity variations. (a) Measured and estimated temperature. (b) Measured humidity.

tag. However, even if variations are observable, it is shown that the measurement can be performed in an inhabited environment, and improvement could be obtained using advanced signal processing.

Last but not least, it is also possible to encapsulate the resonator in a foam-type packaging of few millimetres thick to isolate the effect of humidity from the one of the temperature on the resonator.

XII. Conclusion

This paper introduces an analytical thermal frequency behaviour of resonant scatterers by modelling them as transmission lines. This approach can be generalised to a large variety of resonators as long as their shape can be analytically described using Scattering Matrix concatenation method. The model permits to rigorously link the variations of the measured resonance frequency with the temperature without any lookup table. This can be used to implement the temperature sensing with no additional cost to existing frequency chipless RFID tags while keeping their identification functionality untouched with no modification to implement. Several resonators configurations have been tested (different metals, different substrates, different types of resonator) to validate the equations. Possible applications of this low-cost identification and temperature sensor scatterers can be considered in supplying food, or maintenance.

Acknowledgment

This project has received funding from the European Research Council (ERC) under the European Union's Horizon 2020 research and innovation program (Grant agreement No 772539, ScattererID). This work is also supported by Univ. Grenoble Alpes.

References

[1] E. M. Amin and N. Karmakar, "Development of a chipless RFID temperature sensor using cascaded spiral resonators," in *SENSORS*. IEEE, 2011, pp. 554–557.

[2] R. S. Nair, E. Perret, S. Tedjini, and T. Baron, "A group-delay-based chipless RFID humidity tag sensor using silicon nanowires," *IEEE Antennas Wireless Propag. Lett.*, vol. 12, pp. 729–732, 2013.

[3] C. Occhiuzzi, A. Rida, G. Marrocco, and M. Tentzeris, "RFID passive gas sensor integrating carbon nanotubes," *IEEE Trans. Microw. Theory Techn.*, vol. 59, no. 10, pp. 2674–2684, 2011.

[4] F. Costa, A. Gentile, S. Genovesi, L. Buoncristiani, A. Lazaro, R. Villarino, and D. Girbau, "A depolarizing chipless RF label for dielectric permittivity sensing," *IEEE Microw. Wireless Compon. Lett.*, vol. 28, no. 5, pp. 371–373, 2018.

[5] O. Rance, R. Siragusa, P. Lemaître-Auger, and E. Perret, "Contactless characterization of coplanar stripline discontinuities by RCS measurement," *IEEE Trans. Antennas Propag.*, vol. 65, no. 1, pp. 251–257, 2016.

[6] F. Requena, N. Barbot, D. Kaddour, and E. Perret, "Contactless characterization of metals thermal expansion coefficient by a free-space RF measurement," *IEEE Trans. Antennas Propag.*, 2020.

[7] A. S. Leger and C. Nwankpa, "OTA-based transmission line model with variable parameters for analog power flow computation," *International Journal of Circuit Theory and Applications*, vol. 38, no. 2, pp. 199–220, 2010.

[8] V. Cecchi, A. S. Leger, K. Miu, and C. O. Nwankpa, "Incorporating temperature variations into transmission-line models," *IEEE Trans. Power Del.*", vol. 26, no. 4, pp. 2189–2196, 2011.

[9] J. Virtanen, L. Ukkonen, T. Björninen, L. Sydänheimo, and A. Z. Elsherbeni, "Temperature sensor tag for passive UHF RFID systems," in *Sensors Applications Symposium*. IEEE, 2011, pp. 312–317.

[10] T. Noor, A. Habib, Y. Amin, J. Loo, and H. Tenhunen, "High-density chipless RFID tag for temperature sensing," *Electronics Letters*, vol. 52, no. 8, pp. 620–622, 2016.

[11] S. Preradovic and N. Karmakar, "Chipless RFID tag with integrated sensor," in *SENSORS*. IEEE, 2010, pp. 1277–1281.

[12] A. Vena, L. Sydänheimo, M. M. Tentzeris, and L. Ukkonen, "A fully inkjet-printed wireless and chipless sensor for CO2 and temperature detection," *IEEE Sensors J.*, vol. 15, no. 1, pp. 89–99, 2014.

[13] T. T. Thai, F. Chebila, J. M. Mehdi, P. Pons, H. Aubert, G. R. DeJean, M. M. Tentzeris, and R. Plana, "Design and development of a millimetre-wave novel passive ultrasensitive temperature transducer for remote sensing and identification," in *The 40th European Microwave Conference*. IEEE, 2010, pp. 45–48.

[14] B. Kubina, M. Schüßler, C. Mandel, A. Mehmood, and R. Jakoby, "Wireless high-temperature sensing with a chipless tag based on a dielectric resonator antenna," in *SENSORS*. IEEE, 2013, pp. 1–4.

[15] J. James, J. Spittle, S. Brown, and R. Evans, "A review of measurement techniques for the thermal expansion coefficient of metals and alloys at elevated temperatures," *Measurement science and technology*, vol. 12, no. 3, p. R1, 2001.

[16] Goodfellow.com. (2019). [accessed 28 oct. 2019]. [Online]. Available: http://www.goodfellow.com/PDF/TAB004F.pdf

[17] E. Chen and S. Y. Chou, "Characteristics of coplanar transmission lines on multilayer substrates: Modeling and experiments," *IEEE Trans. Microw. Theory Techn.*, vol. 45, no. 6, pp. 939–945, 1997.

[18] E. Perret, *Radio Frequency Identification and Sensors: From RFID to Chipless RFID*. John Wiley & Sons, 2014.

[19] Rogerscorp.com. (2021). [accessed 04 feb. 2021]. [Online]. Available: https://rogerscorp.com/-/media/project/rogerscorp/documents/advanced-connectivity-solutions/english/data-sheets/ro4000-laminates-ro4003c-and-ro4350b---data-sheet.pdf

[20] Magneticsgroup. (2021). [accessed 04 feb. 2021]. [Online]. Available: https://www.magneticsgroup.com/material/k/

[21] C. A. Balanis, "Advanced Engineering Electromagnetics, John Willey & Sons," *Inc., New York*, 1989.

[22] A. Vena, E. Perret, D. Kaddour, and T. Baron, "Toward a reliable chipless RFID humidity sensor tag based on silicon nanowires," *IEEE Trans. Microw. Theory Tech.*, vol. 64, no. 9, pp. 2977–2985, 2016.